Journal of Radioanalytical and Nuclear Chemistry (2024) 333:2487–2494
https://doi.org/10.1007/s10967-024-09466-x

Numerical study on the characterization of NdFeB permanent magnets with fast-neutrons induced (n, n′γ) reactions

I. Meleshenkovskii[1] · **E. Mauerhofer**[1]

Received: 8 February 2024 / Accepted: 13 March 2024 / Published online: 8 April 2024
© The Author(s) 2024

Abstract
The potential of prompt gamma analysis based on inelastic scattering of 2.5 MeV neutrons for a rapid characterization of NdFeB permanent magnets is investigated by means of numerical simulations using an HPGe detector and a CZT detector-array. The results show that rapid assay of a 42 g magnet can be achieved in some minutes when the neutron flux at sample position is about 1.6×10^9 cm^{-2} s^{-1} and the detector count rate limited to 500 kcps. Such a high neutron flux could be delivered by a compact 5 MeV proton accelerator with a thick beryllium target for neutron production through the ^{9}Be(p,xn)^{9}Be.

Keywords Fast neutron inelastic scattering · Monte Carlo simulations · Prompt gamma-rays · Magnet characterization · Medium resolution detectors

Introduction

Neodymium iron boron NdFeB ($Nd_2Fe_{14}B$) permanent magnets were developed in 1984 and are regarded as the strongest and the best available magnets on the market until today. They are key components in many high technology and consumer products such as electrical and electronics devices, hard-disk drives, sensors, industrial motors, electric and hybrid vehicles, electric bicycles and scooters, wind turbines, medical imaging and scanners. In order to achieve the climate neutrality, the European Union targets a reduction of greenhouse gas emissions by 60% by 2050 [1]. This objective requires an increase of the electricity production from renewable resources like wind and the use of electric or hybrid vehicles which will need around 1–2 million tons and 150,000 tons of permanent magnets, respectively [2]. The rare earth elements (REE) neodymium (Nd), praseodymium (Pr) and dysprosium (Dy) present in NdFeB magnets are classified together with 37 other elements and 9 substances as critical raw materials (CRMs) by the European Commission due to their economic relevance and supply risk [3]. Actions to ensure a secure and sustainable supply of CRMs are proposed in the European Critical Raw Materials Act [4], one of them concerning the recycling. The different strategies and processes for recycling of spent NdFeB magnets and recover of REE like direct recycling and hydrometallurgical, pyrometallurgical and electrochemical extraction are extensively discussed in [5–7]. Efficient recycling requires, at front end, a sorting of the magnets according not only to their type (Ferrite, SmCo, AlNiCo, NFeB, etc.) but also to their content of REEs. A variety of analytical techniques can be used for determination of the REE content in waste flows. Destructive analytical methods, such as Induced Coupled Plasma-Mass/Optical Emission Spectrometry (ICP-MS or -OES) are capable of providing accurate results, necessitating, however, the dissolution of a part of a sample [8]. Moreover, in the case of heterogeneous samples, the results are not representative for the whole sample. X-Ray Fluorescence (XRF) [9] and Laser Induced Breakdown Spectroscopy (LIBS) [10] are non-destructive methods but provide only near-surface information and are not able to identify stacks of materials. Prompt Gamma Neutron Activation analysis (PGNAA) technique with cold or thermal neutrons reaches its performance capabilities due to penetration length limitations of the incident neutron beam in dense materials [11, 12]. Besides, the use of cold neutrons requires complicated instrumentation and is thus not suitable for in-situ industrial applications. Neutron Activation Analysis (NAA) requires access to a research reactor, which, coupled with

✉ I. Meleshenkovskii
i.meleshenkovskii@fz-juelich.de

[1] Jülich Centre for Neutron Science, Forschungszentrum Jülich GmbH, 52425 Jülich, Germany

the timelines of such measurements, is not suitable for the task either. As a result, absence of a consistent and straightforward solution to characterize rapidly all types of magnets and unfold qualitative and quantitative information about the elemental composition of REEs is a critical issue for the magnet recycling industry.

Prompt Gamma Analysis based on Inelastic Neutron Scattering (PGAINS) could be suitable for a rapid determination of the elemental composition of permanent magnets. This method measures the element specific gamma-rays induced by the inelastic scattering of fast neutrons i.e. (n,n′γ) reactions. It may be mentioned here that the energies of these gamma-rays differ from the energies of the gamma-rays produced by neutron capture reactions. The proof of principle of PGAINS has been demonstrated with the FaNGaS (Fast Neutron-induced Gamma-ray Spectrometry) instrument installed at Heinz Maier-Leibnitz Zentrum (MLZ) using the intense fission neutron beam delivered by the beamtube SR 10 of the FRM II reactor (Forschungs-Neutronenquelle Heinz Maier-Leibnitz) [13–17]. In this work, we investigate the detection of neodymium and dysprosium in NdFeB magnet samples by means of numerical simulations in PHITS code using a beam of 2.5 MeV neutrons. The gamma-ray spectra are collected either with a high-resolution HPGe-detector with 50% efficiency or an array of 8 cadmium zinc telluride (CZT) detectors. The results obtained for the two detection systems are used to estimate the basic parameters and counting times for the development of a real measurement system and to perform further optimization of the numerical model in terms of geometrical configuration of the measurement cell and shielding.

Numerical simulation

The numerical simulations are performed with the PHITS code (Particle and Heavy Ion Transport code System, version 3.28) [18] using the JENDL-4.0 [19] nuclear data library. The geometry of the simulation environment is shown in Fig. 1. A disc-shaped magnet sample with a diameter of 2.8 cm and a thickness of 1 cm is fully irradiated with a parallel beam of 2.5-MeV neutrons of same diameter as the sample. The prompt gamma-ray spectra are collected with a high-resolution HPGe detector (Fig. 1) or with an array of 8 cadmium zinc telluride (CZT) detectors (Fig. 1) positioned at 90° relatively to the axis of the neutron beam and close to the sample. The short sample-to-detector distance allows for collecting gamma-ray spectra with a high counting statistics and does not correspond at this point to a real system because of the detector-preamplifier saturation due to very high input count rates. No shielding material is placed between detector and neutron beam. The HPGe detector is analog to that of the FaNGaS spectrometer (50% relative efficiency, energy resolution of 2.2 keV at 1.33 MeV) and simply modelled by a cylindrical germanium crystal with a length of 8.5 cm and a diameter of 6.4 cm. The CZT detector-array is composed of two arrays of 4 CZT detectors placed on each side of the sample. Each individual CZT detector has a surface of 4×4 cm^2 and a thickness of 1.5 cm. The energy resolution is 2.5% at 661 keV [20]. The distance between the center of the sample and detector surface is 2 cm for the HPGe-detector and 2.4 cm for each CZT-detector. The spectra are collected with 16,384 energy bins and the upper energy threshold set to 9000 keV. Simulations are conducted for NdFeB magnet samples with various neodymium and

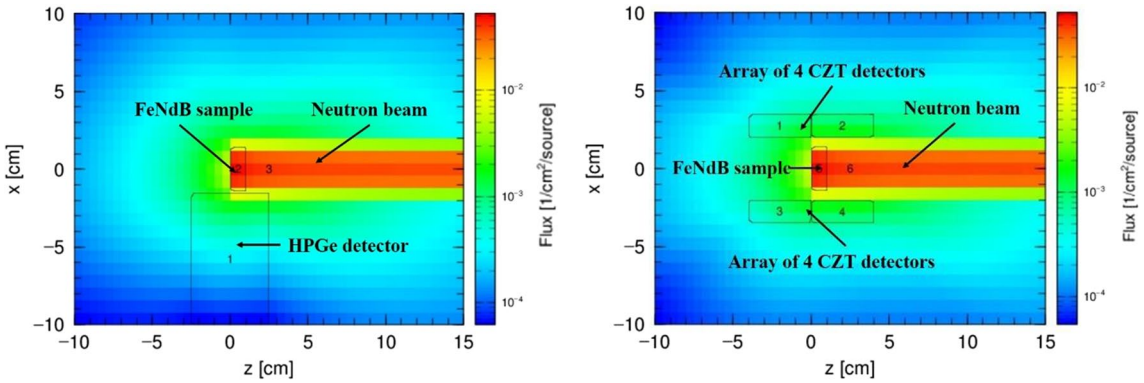

Fig. 1. 2D view of the PHITS simulation model with the HPGe detector (left) and with the CZT detector-array composed of two arrays of 4 CZT detectors placed on each side of the sample (right) showing the distribution of the neutron fluence in middle plane of the neutron beam

Table 1 Elemental composition of FeNdB magnets according to [21, 25]

Element	Comp1	Comp2	Comp3	Comp4	Comp5	Comp6
Fe	67%	67%	67%	67%	67%	67%
Nd	30.6%	29.2%	27.9%	25.6%	23.3%	21.9%
Dy	1.4%	2.8%	4.1%	6.4%	8.7%	10.1%
B	1%	1%	1%	1%	1%	1%

The density of the material that varies slightly with the magnet composition is 7.6 g cm^{-3}

dysprosium contents (Table 1). The number of primary neutrons is 10^{10} for each simulation corresponding to a neutron fluence of 1.62×10^{9} cm^{-2} at sample position. The simulated spectra are analyzed with the spectroscopy software Gamma-W (Westmeier GmbH).

Results

Parts of the simulated spectra of the magnet samples with different neodymium and dysprosium contents are shown in Fig. 2. The production of gamma-rays from fast neutron capture reactions is negligible due to lower cross-sections compared to the (n,n′) reactions. Assignment of the gamma-ray energies which are due to inelastic scattering of fast neutrons to the isotopes is done using data given in [21] and the database NuDat 3.0 [22]. The most intense signature lines of dysprosium, neodymium and iron are labelled in the spectra. Based on the spectra of the HPGe detector, the following interference-free lines are selected: 454 keV (^{146}Nd), 1377 keV (^{144}Nd, ^{146}Nd) and 1575 keV (^{142}Nd) for neodymium, 167 keV (^{161}Dy, ^{163}Dy), 169 keV (^{164}Dy), and 185 keV (^{162}Dy) for dysprosium and 846 keV (^{56}Fe) for iron. In the case of the CZT detector-array, the lines at 167 and 169 keV are not resolved, forming a single peak containing also a contribution of the 165-keV line of ^{163}Dy. The same is observed for the 185-keV line with a contribution of the weak line of ^{161}Dy at 183 keV. The peak at 454 keV includes a contribution of the 448- and 451-keV lines of ^{146}Nd and^{148}Nd, respectively. The net count rates of the aforementioned lines normalized to a neutron emission of 10^{10} s^{-1} are given for the HPGe and CZT detector-array in Tables 2 and 3, respectively. The linear relationship between count rate and element mass is shown in Fig. 3 and the resulting correlation coefficients are given in column 9 of Tables 2 and 3. Due to the close distance between sample and detector the total count rate for both detectors is 3×10^{8} s^{-1} for a neutron flux and sample position of 1.62×10^{9} cm^{-2} s^{-1}. This corresponds to the total count rate of 3.8×10^{7} s^{-1} for each CZT detector equipped with its own readout electronics for signal processing.

Discussion

Based on the simulation results a rapid determination of neodymium and dysprosium content in FeNdB magnets requires a high fast neutron flux at sample position in conjunction with an optimal sample-to-detector distance in order to avoid saturation of detector electronics. Let′s first consider as 2.5 MeV neutron source a deuterium-deuterium neutron generator with a neutron emission of $N_0=10^{10}$ s^{-1} in 4pi. For a distance between neutron source and sample of $L=30$ to 50 cm for example (some optimized shielding material is needed between the neutron source and the detector in the real measurement system [21]) the neutron flux at sample position will be between 3×10^{5} and 9×10^{5} cm^{-2} s^{-1} ($N_0/4\pi L^2$). It means that for reaching the gamma-ray counts obtained in the simulation with a flux of 1.6×10^{9} cm^{-2} s^{-1} and the close sample-to-detector distance a counting time of between 30 and 90 min will be necessary. This assay time is definitively too long for a characterization of magnets at industrial scale which requires a high sample throughput. An intense fast neutron flux at sample position could be delivered by a compact accelerator based neutron source (CANS) composed of a 5 MeV proton accelerator and a thick beryllium neutron-target. In this case the ^{9}Be(p, xn)^{9}Be reaction produces a total neutron yield of 3.5×10^{12} mA^{-1} s^{-1} in 4π sr [22]. At an angle of 0° with respect to the proton beam, the neutron spectrum has a maximum at 2.7 MeV and the neutron yield is 4×10^{11} mA^{-1} s^{-1} [22]. Thus, setting the proton beam current to 25 µA will offer a neutron emission of 10^{10} s^{-1} towards the sample and a flux at sample position of 1.62×10^{9} cm^{-2} s^{-1} corresponding to the parameters used in the simulations. In order to avoid saturation of the detector preamplifier the distance between sample and detector must be increase compared to the close counting geometry of the simulations. The total detector count rate decreases by a factor defined as the ratio of the solid angles subtended by the detector at the sample position, $\Omega(d)/\Omega$ (d_0) calculated for the new distance d and the distance d_0 set in the simulations.

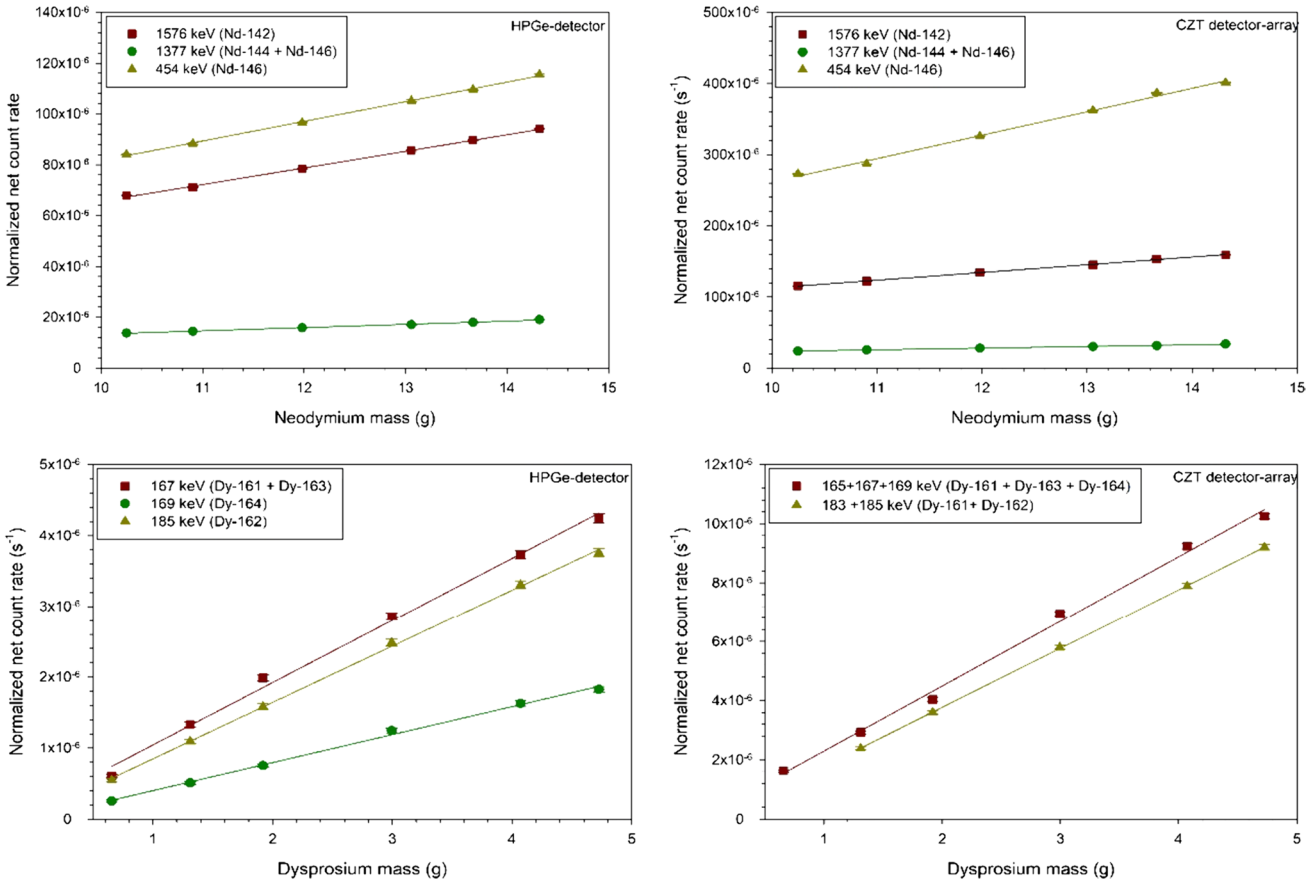

Fig. 2 Linear relationship between the normalized count rates of selected neodymium and dysprosium lines and the element mass for the HPGe-detector (left) and the CZT detector-array (right). The count rates are normalized to a neutron emission of 10^{10} s^{-1}

For the HPGe detector d_0 is 2.4 cm and $\Omega(d_0) = 2.51$ sr. For each CZT detector-array, d_0 is 2 cm and $\Omega(d_0) = 3.71$ sr. For simplification, the solid angle is calculated assuming the sample as a point source. The inverse value of the solid angle ratio corresponds to the counting time t_c needed to obtain the same spectra as the simulated ones i.e. the count rates of the gamma lines given in Tables 2 and 3. The values of d, $\Omega(d)$, and t_c obtained for total detector count rate of 250 kcps, 500 kcps and 1000 kcps are given in Table 4. Such high-count rates can be handle without considerable degradation of the energy resolution with the adaptive digital pulse processing system including pulse deconvolution developed in [23]. As seen from Table 4, the CZT detector array due to its better geometrical efficiency requires less time to characterize a 42 g NdFeB magnet sample than the HPGe-detector, one main limiting factor for the latter being the input count rate. However, with a better energy resolution HPGe-detectors offers a lower limit of detection. One advantage of CZT detectors is that they are room temperature devices and do not require cooling unlike HPGe detectors. Moreover, recent progress and development in CZT detector technology opens a promising future for application of CZT detectors for such analytical tasks, offering an energy resolution better than 1% at 662 keV [24]. Of course, the time required to characterize a magnet will depend on its mass, size or shape i.e. on its neutron self-shielding and gamma self-absorption and further numerical simulations must be carried out to optimize such as analytical system including also the neutron- and gamma-shielding components.

Conclusions

In this work, we explored the possibility of a rapid characterization of NdFeB permanent magnets in view of their sorting/recycling at industrial scale simulating the measurement of prompt gamma-rays induced by inelastic scattering of 2.5 MeV neutrons with the PHITS code. Magnets (mass: 42 g) with various neodymium and dysprosium content were irradiated with an intense neutron beam (10^{10} s^{-1}) and the gamma-ray spectra recorded with two different detectors, a HPGe detector and two CZT detector-arrays placed close to the sample. For both detectors a very good linear relationship was obtained between the count rates of selected gamma lines of neodymium and dysprosium and the element mass. A rapid characterization of the magnets (interrogation time of about 1 min or less) requires a high neutron flux at sample position that cannot be achieved by using a deuterium-deuterium neutron generator with a neutron emission of 10^{10} s^{-1} 4π sr. In this case, the time needed to characterize a magnet ranges between 30 and 90 min for a small sample-to-detector distance. A high sample neutron flux can be delivered by a CANS based on a 5 MeV proton accelerator and a thick beryllium target for neutron production via the $^{9}B(p,xn)^{9}Be$ reaction. With such a neutron source and limiting the input count rate to 500 kcps the characterization of a 42 g magnet could be attained in 6 min with the HPGe detector (distance from sample: 88 cm) and in 1.3 min with the CZT detector-arrays (distance from sample: 36 cm) composed of 8 individual CZT detectors with own readout electronics. The results show the promising potential of the PGAINS technique using a CANS for rapid characterization of magnets of various types and other materials in industrial

Table 2 Net count rate of neodymium, dysprosium and iron lines C normalized to a neutron emission of 10^{10} s^{-1} neutrons obtained for the HPGe-detector

		C [s^{-1}]×10^{-5}						R	C_{spe} [s^{-1} g^{-1}]×10^{-6}
Eγ [keV]	Isotope	Comp1	Comp2	Comp3	Comp4	Comp5	Comp6		
Neodymium:		**14.32 g**	**13.66 g**	**13.06 g**	**11.98 g**	**10.90 g**	**10.25 g**		
454	^{146}Nd	11.55(3)	10.96(3)	10.52(3)	9.66(3)	8.82(3)	8.41(3)	0.999	8.05(6)
1377	^{144}Nd,^{146}Nd	1.90(1)	1.79(1)	1.71(1)	1.58(1)	1.44(1)	1.11(1)	0.998	1.32(1)
1575	^{142}Nd	9.40(3)	8.97(3)	8.55(3)	7.84(3)	7.11(3)	6.78(2)	0.999	6.56(3)
Dysprosium:		**0.65 g**	**1.31 g**	**1.92 g**	**2.99 g**	**4.07 g**	**4.72 g**		
167	^{161}Dy,^{163}Dy	0.061(2)	0.133(3)	0.198(4)	0.286(5)	0.773(6)	0.425(6)	0.997	0.96(4)
169	^{164}Dy	0.025(2)	0.051(2)	0.075(3)	0.124(3)	0.163(4)	0.182(4)	0.998	0.39(1)
185	^{162}Dy	0.054(2)	0.109(3)	0.158(4)	0.248(5)	0.331(5)	0.375(6)	0.999	0.82(2)
Iron:		**31.35 g**	**31.35 g**	**31.35 g**	**31.35 g**	**31.35 g**	**31.35 g**		
846	^{56}Fe	73.06(3)	72.79(3)	72.69(3)	72.60(3)	72.24(3)	73.47(3)	–	23.2(1)

Bold the indicate values make it easier to distinguish between the results for different materials and samples

Comp means Composition

C_{spe} is the count rate per gram of element. R is the coefficient of correlation of the linear relationship between count rate and element mass

Table 3 Net count rate of neodymium, dysprosium and iron lines C normalized to a neutron emission of 10^{10} s^{-1} neutrons obtained for the CZT detector-array

		C [s^{-1}]×10^{-5}						R	C_{spe} [s^{-1} g^{-1}]×10^{-6}
E_γ [keV]	Isotope	Comp1	Comp2	Comp3	Comp4	Comp5	Comp6		
Neodymium:		**14.32 g**	**13.66 g**	**13.06 g**	**11.98 g**	**10.90 g**	**10.25 g**		
448 + 451 + 454	^{146}Nd,^{148}Nd,^{146}Nd	40.09(6)	38.67(6)	36.21(6)	32.57(5)	28.66(5)	27.29(5)	0.998	27.35(8)
1377	^{144}Nd,^{146}Nd	3.36(2)	3.15(2)	3.03(2)	2.78(2)	2.54(2)	2.38(1)	0.999	2.32(1)
1575	^{142}Nd	15.91(4)	15.32(4)	14.50(4)	13.45(3)	12.20(3)	11.53(3)	0.999	11.18(6)
Dysprosium:		**0.65 g**	**1.31 g**	**1.92 g**	**2.99 g**	**4.07 g**	**4.72 g**		
165 + 167 + 169	^{161}Dy,^{163}Dy,^{164}Dy	0.162(12)	0.293(5)	0.403(6)	0.694(8)	0.923(9)	1.02(1)	0.998	2.3(1)
183 + 185	^{161}Dy,^{162}Dy	ND	0.238(5)	0.360(6)	0.580(7)	0.789(8)	0.920(9)	1.000	1.90(6)
Iron:		**31.35 g**	**31.35 g**	**31.35 g**	**31.35 g**	**31.35 g**	**31.35 g**		
846	^{56}Fe	158.3(1)	151.4(1)	152.4(1)	154.2(1)	154.8(1)	154.9(1)	-	49.2(8)

C_{spe} is the count rate per gram of element. R is the coefficient of correlation of the linear relationship between count rate and element mass

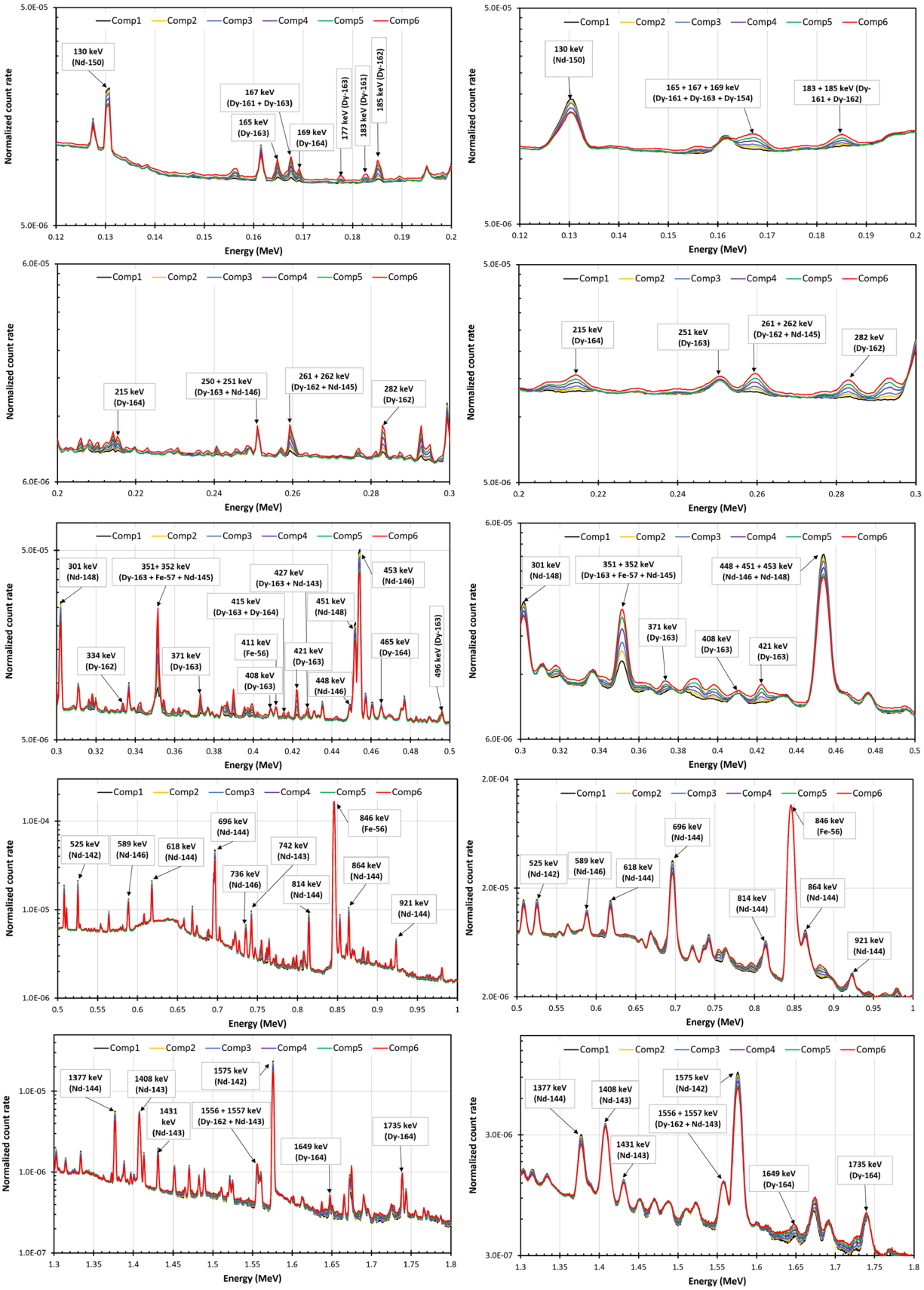
Comp1 Comp2 Comp3 Comp4 Comp5 Comp6
Normalized count rate
Energy (MeV)
130 keV (Nd-150)
167 keV (Dy-161 + Dy-163)
165 keV (Dy-163)
169 keV (Dy-164)
177 keV (Dy-163)
183 keV (Dy-161)
185 keV (Dy-162)
165 + 167 + 169 keV (Dy-161 + Dy-163 + Dy-154)
183 + 185 keV (Dy-161 + Dy-162)
215 keV (Dy-164)
250 + 251 keV (Dy-163 + Nd-146)
261 + 262 keV (Dy-162 + Nd-145)
282 keV (Dy-162)
251 keV (Dy-163)
301 keV (Nd-148)
351+ 352 keV (Dy-163 + Fe-57 + Nd-145)
427 keV (Dy-163 + Nd-143)
453 keV (Nd-146)
415 keV (Dy-163 + Dy-164)
451 keV (Nd-148)
411 keV (Fe-56)
421 keV (Dy-163)
465 keV (Dy-164)
496 keV (Dy-163)
334 keV (Dy-162)
371 keV (Dy-163)
408 keV (Dy-163)
448 keV (Nd-146)
351 + 352 keV (Dy-163 + Fe-57 + Nd-145)
448 + 451 + 453 keV (Nd-146 + Nd-148)
525 keV (Nd-142)
589 keV (Nd-146)
618 keV (Nd-144)
696 keV (Nd-144)
742 keV (Nd-143)
846 keV (Fe-56)
736 keV (Nd-146)
814 keV (Nd-144)
864 keV (Nd-144)
921 keV (Nd-144)
1377 keV (Nd-144)
1408 keV (Nd-143)
1575 keV (Nd-142)
1431 keV (Nd-143)
1556 + 1557 keV (Dy-162 + Nd-143)
1649 keV (Dy-164)
1735 keV (Dy-164)

◂**Fig. 3** Parts of the simulated prompt gamma-ray spectra of magnet samples with different compositions (see Table 1) for the HPGe detector (left) and the CZT detector-array (right). The count rate is normalized to a neutron emission of 10^{10} s^{-1}

Table 4 Counting time t_c required to generate the spectra simulated for a 42 g magnet with a neutron flux of 1.62×10^9 cm^{-2} s^{-1} at various sample-to-detector distances d i.e. various total detector count rates C_{total}

C_{total} (kcps)	HPGe detector			CZT detector arrays		
	d (cm)	Ω(d) (sr)	t_c (min)	*d* (cm)	Ω(*d*) (sr)	tc (min)
250	124	$2.09\ 10^{-3}$	20	45	$3.09\ 10^{-2}$	2
500	88	$4.18\ 10^{-3}$	6	36	$4.88\ 10^{-2}$	1.3
1000	62	$8.38\ 10^{-3}$	2	25	$9.77\ 10^{-2}$	0.6

Ω(*d*) is the solid angle subtended by the detector. Note that for the CZT detector-arrays C_{total} corresponds to the total count rate of each single CZT detector in the array

applications. However, further studies based on numerical simulations are necessary for the design of a real system, including the dynamical range of sample masses that could be assayed, the neutron beam size, the irradiation chamber with neutron beam stop, the neutron and gamma shielding and the optimization of the detector geometry according to the input count rate.

Acknowledgements This project has received funding from the European Union's Horizon 2020 Research and Innovation Programme under the Marie Skłodowska-Curie Grant Agreement N°101034266. The authors would like to thank Dr. Tatsuhiko Ogawa for his help with cluster simulations.

Funding Open Access funding enabled and organized by Projekt DEAL.

Declarations

Conflict of interest The authors have no competing interests to declare that are relevant to the content of this article.

Data availability All metadata presented in this article are stored at Jülich Centre for Neutron Science, Forschungszentrum Jülich GmbH.

Open Access This article is licensed under a Creative Commons Attribution 4.0 International License, which permits use, sharing, adaptation, distribution and reproduction in any medium or format, as long as you give appropriate credit to the original author(s) and the source, provide a link to the Creative Commons licence, and indicate if changes were made. The images or other third party material in this article are included in the article's Creative Commons licence, unless indicated otherwise in a credit line to the material. If material is not included in the article's Creative Commons licence and your intended use is not permitted by statutory regulation or exceeds the permitted use, you will need to obtain permission directly from the copyright holder. To view a copy of this licence, visit http://creativecommons.org/licenses/by/4.0/.

References

1. Commission E (2019) The European Green Deal. Eur Commun 53:24
2. Nakamura H (2018) The current and future status of rare earth permanent magnets. Scr Mater 154:273–276
3. European Commission. Directorate-General for Internal Market, Industry, Entrepeneurship and SMEs, Blengini GA, EL Latunussa C, Eynard U, Torres de Matos C, Wittmer D, Georgitzikis K, Pavel C, Carrara S, Mancini L, Unguru M, Blagoeva D, Mathieux F, Pennington.(2020) D Study on the EU's list of Critical Raw Materials (2020) Final Report, Publications office, https://data.europa.eu/doi/https://doi.org/10.2873/11619
4. European Commission - Press release. Critcal Raw Materials: ensuring secure and sustainable supply chains foe EU′s green and digital future, Brussels, 16 March 2023. https://ec.europa.eu/commission/presscorner/detail/en/ip_23_1661
5. Yang Y, Walton A, Sheridan R, Güth K, Gauß R, Gutfleisch O, Buchert M, Steenari B-M, Van Gerven T, Jones PT, Binnemans K (2017) REE recovery from end-of-life NdFeB permant magnetr scrap: a critical review. J Sustain Metall 3:122–149
6. Becci A, Beolchini F, Amato A (2021) Sustainable strategies for exploitation of end-of-life permanemts magnets. Processes 9:857
7. Kumari A, Sahu SK (2023) A comprehensivew review on recycling of critical rwa materials from spent neodymium iron boron (NdFeB) magnet. Sep Purif Technol 317:123527
8. Korotkova NA, Baranovskaya VB, Petrova KV (2022) Microwave digestion and ICP-MS determination of major and trace elements in waste Sm-Co magnets. Metals 12:1308
9. Castro JP, Speranca MA, Babos DV, Andrade DF, Pereira-Filho ER (2020) Neodynium determination in hard drive disks magnets using different calibration approaches for wavelenth dispersive X-ray fluorescence. Spectrochim Acta, Part B 164:105763
10. Castro JP, Speranca MA, Babos DV, Andrade DF, Pereira-Filho ER (2020) Calibration strategies for th direct determination of rare earth elements in hard disks magnets using laser-induced breakdown spectroscopy. Talanta 208:120443
11. Blaauw M, Degenaar I, Yonezawa C, Matsue H, de Goeij J (2007) Development of non-invasive method for the determination of the macroscopic neutron cross sections of a sample matrix in large-sample prompt gamma neutron activation analysis. J Radioanal Nucl Chem 3:765–770

12. Blaauw M, Belgya T (2005) Neutron self-shielding correction for prompt gamma neutron activation analysis of large samples. J Radioanal Nucl Chem 265:257–259
13. Ilic Z, Mauerhofer E, Stieghorst C, Révay Z, Rossbach M, Randriamalala TH, Brückel T (2020) Prompt gamma rays incuced by inelastic scattering of fission neutrons on iron. J Radioanal Nucl Chem 325:641–645
14. Mauerhofer E, Ilic Z, Stieghorst C, Zs R, Rossbach M, Li J, Randriamalala TH, Brückel T (2021) Prompt and delayed gamma rays induced by epithermal and fast neutrons with indium. J Radioanal Nucl Chem 331:535–546
15. Mauerhofer E, Ilic Z, Stieghorst C, Zs R, Vezhlev E, Ophoven N, Randriamalala TH, Brückel T (2022) Prompt gamma rays from fast neutron inelastic scattering on aluminum, titanium and copper. J Radioanal Nucl Chem 331:3987–4000
16. Ophoven N, Ilic Z, Mauerhofer E, Randriamalala TH, Vezhlev E, Stieghorst C, Zs R, Brückel T, Jolie J, Strub E (2022) Fast neutron induced gamma rays from (n, n'), (n, p) and (n, α) reactions on CaCO3. J Radioanal Nucl Chem 331:5729–5740
17. Ophoven N, Ilic Z, Mauerhofer E, Randriamalala TH, Vezhlev E, Stieghorst C, Révay Zs, Brückel T, Jolie J, Strub E (2023) Prompt gamma rays from fast neutron induced reactions on cerium and chlorine. J Radioanal Nucl Chem 332:3133–3145
18. Sato T, Iwamoto Y, Hashimoto S, Ogawa T, Furuta T, Abe S, Kai T, Tsai PE, Matsuda N, Iwase H, Shigyo N, Sihver L, Niita K (2018) Features of particle and heavy ion transport code system PHITS version 3.02. J Nucl Sci Technol 55:684–690
19. Shibata K, Iwamoto O, Nakagawa T, Iwamoto N, Ichihara A, Kunedia S, Chiba S, Furutaka K, Otuka N, Murata T, Matsunobu H, Zukeran A, Kamada S, Kataruka J-I (2012) ENDL-40 A new library for nuclear science and engineering. J Nucl Sci Technol 8(1):1–30
20. Meleshenkovskii I, Ogawa T, Pauly N, Labeau P-E (2020) A novel asymmetrical peak broadening feature for a CdZnTe detector response function modeling using PHITS particle and heavy ion transport simulation code. Nucl Instru Meth Sect B 467:108–113. https://doi.org/10.1016/j.nimb.2020.02.014
21. Yun S, Woo Lee C, Won Lee D, Kim SH, Jung B, Chang DF, Jin HG, Shin CW (2019) An optimization study for shielding design of D-D and D-T neutrongenerators. Fusion Eng Des 146:531–534
22. Agosteo A, Colautti P, Esposito J, Fazzi A, Introini MV, Pola A (2011) Characterization of the energy distribution of neutrons generated by 5 MeV protons on a thick beryllium target at different emission angles. Appl Radiat Isot 69:1664–1667
23. Saxena S, Hawari AI (2020) Digital pulse deconvolution with adaptive shaping for real-time high-resolution high-throughput gamma spectroscopy. Nucl Instr Methods Phys Res Sect A Accel Spectro Detect Assoc Equip 954:161288. https://doi.org/10.1016/j.nima.2018.09.123
24. Abbene L, Principato F, Buttacavoli A, Gerardi G, Bettelli M, Zappettini A, Altieri S, Auricchio N, Caroli E, Zanettini S et al (2022) Potentialities of high-resolution 3-D CZT drift strip detectors for prompt gamma-ray measurements in BNCT. Sensors 22(4):1502. https://doi.org/10.3390/s22041502
25. Working Paper Sustainability and Innovation No. S 05/2016, Simon GLÖSER-CHAHOUD, André KÜHN, Luis TERCERO ESPINOZA, Globale Verwendungsstrukturen der Magnetwerkstoffe Neodym und Dysprosium: Eine szenariobasierte Analyse der Auswirkung der Diffusion der Elektromobilität auf den Bedarf an Seltenen Erden, Fraunhofer ISI, Karlsruhe, Juni 2016

Publisher's Note Springer Nature remains neutral with regard to jurisdictional claims in published maps and institutional affiliations.